ISSN 0036-0244, Russian Journal of Physical Chemistry A, 2019, Vol. 93, No. 11, pp. 2197–2202. © Pleiades Publishing, Ltd., 2019.

PHYSICAL CHEMISTRY OF SOLUTIONS

Solid–Liquid Phase Equilibrium in Aqueous Quaternary System Li^+,Rb^+,Mg^{2+}//Borate–H_2O at $T = 323$ K

Xudong Yu[a,b,*], Maolan Li[a], Qiufeng Zheng[a], Ying Zeng[a,b], and Feihong Guo[a]

[a] *College of Materials and Chemistry and Chemical Engineering, Chengdu University of Technology, Chengdu, 610059 P. R. China*

[b] *Collaborative Innovation Center of Panxi Strategic Mineral Resources Multi-Purpose Utilization (Chengdu University of Technology), Chengdu, 610059 P. R. China*

**e-mail: xwdlyxd@126.com*

Received October 16, 2018; revised December 25, 2018; accepted January 15, 2019

Abstract—The stable phase equilibria, densities, and refractive indices of the aqueous quaternary system Li^+,Rb^+,Mg^{2+}//borate–H_2O at 323 K were determined by the isothermal dissolution method. It was found that the phase diagram consists of one quaternary invariant point, two isothermal dissolution curves, and three fields of crystallization corresponding to three single salts $Li_2B_4O_7 \cdot 3H_2O$, $MgB_4O_7 \cdot 9H_2O$, and $RbB_5O_8 \cdot 4H_2O$, respectively. The size of crystallization regions of salt decreased in the order $MgB_4O_7 \cdot 9H_2O$ > $RbB_5O_8 \cdot 4H_2O$ > $Li_2B_4O_7 \cdot 3H_2O$. The comparison of phase diagrams of the system at 298–348 K shown that the crystalline form of salts lithium borate, magnesium borate, and rubidium borate did not change at 298–348 K. The crystalline area of $MgB_4O_7 \cdot 9H_2O$ is the largest than that of 298 and 348 K. The crystalline area of $RbB_5O_8 \cdot 4H_2O$ is the smallest than that of 298 and 348 K, while the crystalline are of $Li_2B_4O_7 \cdot 3H_2O$ is larger than that of 298 K, and smaller than that of 348 K.

Keywords: borate, solubility, rubidium, magnesium, hydrate salt

DOI: 10.1134/S0036024419110359

1. INTRODUCTION

Phase equilibrium of borate containing system is important because there are various forms of boron such as $B(OH)_3$, BO_2^-, $B(OH)_4^-$, $B_4O_5(OH)_4^{2-}$ appeared in the solution [1]. Therefore the solubility isotherms and thermodynamics properties of the borates in pure liquids within multiple temperatures are of significant importance for extracting borates from salt lake and underground brines. For this reason, the phase equilibria of the aqueous systems or subsystems composed of lithium, potassium, sodium, magnesium, rubidium, and borate were done by previous research [2–11].

As for the system Li^+,Rb^+,Mg^{2+}//borate–H_2O studied in this article, the corresponding phase diagrams at 298 and 348 K have been completed by our research group [12, 13], while the solid-liquid equilibrium of system Li^+,Rb^+,Mg^{2+}//borate–H_2O at 323 K has not been carried out. Consequently, on the basis of results for ternary subsystems, the phase equilibrium of system Li^+,Rb^+,Mg^{2+}//borate–H_2O at 323 K is reported in detail.

2. EXPERIMENTAL

2.1. Materials

All solutions were prepared using the doubly deionized water, which was obtained using a Millipore water system with an electrical conductivity less than 5.5×10^{-6} S m^{-1}. Lithium tetraborate anhydrous ($Li_2B_4O_7$), magnesium oxide (MgO), and boric acid (H_3BO_3) were obtained from Chengdu Kelong Chemical Reagent Plant with purity of 99.5%. Rubidium carbonate (Rb_2CO_3) was obtained from Jiangxi Dongpeng New Materials Co., Ltd. with purity of 99.5%. Rubidium pentaborate ($RbB_5O_6(OH)_4 \cdot 2H_2O$) and Hungtsaoite ($MgB_4O_5(OH)_4 \cdot 7H_2O$) with purity higher than 99.0% were synthesized in our laboratory [14, 15].

2.2. Methods and Apparatus

The isothermal dissolution method was applied to the phase equilibrium experiments [2]. A series of samples with different amounts of $Li_2B_4O_7$, $MgB_4O_7 \cdot 9H_2O$, $RbB_5O_8 \cdot 4H_2O$, and H_2O were put into 100 mL tightly sealed bottles, immersed in the THZ-82 type thermostatic shaker with 120 rpm speed at (323 ± 0.2) K,

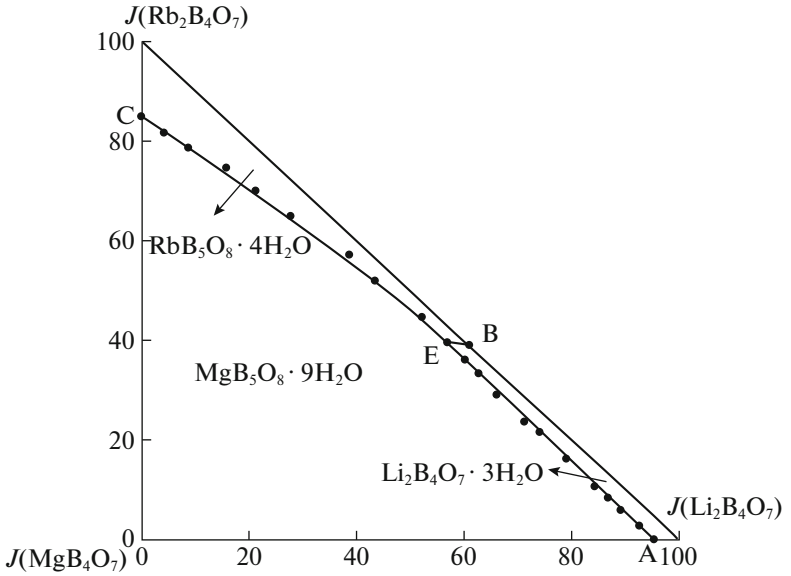

Fig. 1. Phase diagram of the quaternary system Li^+,Rb^+,Mg^{2+}//borate–H_2O at 323 K.

once the content of liquid phase became constant, it indicated that the equilibrium had been reached. And then, the liquid and solid phases were separated by filtration at 323 K. The densities of the solution at equilibrium were determined by the gravity bottle method [16], and the refractive indices of the equilibrated solution were measured with the Abbe refractometer (WYA type, Shanghai Precision & Scientific Instrument Co., Ltd.); meanwhile a certain amount solution was diluted to a final volume of 250 mL for analysis the compositions. The wet solids were dried at 323 K and characterized using X-ray diffraction (DX-2700 type, Dandong Fangyuan Instrument Co., Ltd.).

3. ANALYTICAL METHODS [17, 18]

Li^+: ICP-OES, with standard uncertainty of 0.50%;

Rb^+: sodium tetraphenylborate (STPB)—hexadecyltrimethylammonium bromide ($C_{19}H_{42}BrN$) back titration method, with standard uncertainty of 0.50%;

Borate: neutralization titration in the presence of mannitol with standard uncertainty of 0.30%;

Mg^{2+}: titration with EDTA standard solution, standard uncertainty of 0.50%.

4. RESULTS AND DISCUSSION

The experimental data for the aqueous quaternary system Li^+,Rb^+,Mg^{2+}//borate–H_2O at 323 K are given in Table 1. Commonly, $B_4O_7^{2-}$ represents all kinds of possibly existing forms of boron ions in the solution. Thus, the crystalline form of salt was described as $RbB_5O_8 \cdot 4H_2O$ and $B_4O_7^{2-}$ is used to express the different boric species in solution, therefore, $Rb_2B_4O_7$ was indicated in Table 1.

The phase diagram of system Li^+,Rb^+,Mg^{2+}//borate–H_2O at 323 K was plotted as shown in Fig. 1. The phase diagram consists of one quaternary invariant point, three isothermal dissolution curves, and three crystalline zones. The composition of the solid phase in point E was analyzed by the X-ray diffraction method and the XRD pattern was given in Fig. 2. The identification is performed by comparison of the diffraction pattern to databases showing that salts $Li_2B_4O_7 \cdot 3H_2O$ (PDF no. 50-0564), $RbB_5O_8 \cdot 4H_2O$ (PDF no. 43-0415), and $MgB_4O_7 \cdot 4H_2O$ (PDF no. 34-1288) coexist in the invariant point E. The liquid composition of point E is $w(Li_2B_4O_7) = 3.63\%$, $w(Rb_2B_4O_7) = 4.87\%$, $w(MgB_4O_7) = 0.25\%$, and $w(H_2O) = 91.25\%$.

Among the three crystalline regions, the crystallization areas of the salts are in the following order: $MgB_4O_7 \cdot 9H_2O > RbB_5O_8 \cdot 4H_2O > Li_2B_4O_7 \cdot 3H_2O$, which means that the solubility of $Li_2B_4O_7$ is the largest.

The comparison of the phase diagram (Fig. 3) of system Li^+,Rb^+,Mg^{2+}//borate–H_2O between 298 [12], 323 and 348 K [13] shows that (1) the crystalline form of salts lithium borate, magnesium borate, and rubidium borate did not change at 298–348 K; (2) the crystalline of $MgB_4O_7 \cdot 9H_2O$ is the largest than that of

Table 1. The solid–liquid equilibrium and physicochemical properties (Density and Refractive index) of the quaternary system Li^+,Rb^+,Mg^{2+}//borate–H_2O at 323 K and pressure $p = 0.1$ MPa[a]

No.	Density, g m^{-3}	Refractive index, n_D	Equilibrium solutions composition, $w(B) \times 10^2$				Jänecke index of dry salt $J(Li_2B_4O_7) + J(Rb_2B_4O_7) + J(MgB_4O_7) = 100$				Equilibrium solid phase
			$w(Li_2B_4O_7)$	$w(Rb_2B_4O_7)$	$w(MgB_4O_7)$	$w(H_2O)$	$J(Li_2B_4O_7)$	$J(Rb_2B_4O_7)$	$J(MgB_4O_7)$	$J(H_2O)$	
1, A	1.0831	1.3418	4.53	0.00	0.23	95.24	95.44	0.00	4.56	18830	LiB + MB
2	1.0835	1.3427	4.48	0.25	0.24	95.03	92.64	2.69	4.67	18442	LiB + MB
3	1.0849	1.3445	4.35	0.54	0.26	94.85	89.23	5.74	5.03	18260	LiB + MB
4	1.0854	1.3459	4.21	0.78	0.25	94.76	86.80	8.34	4.86	18336	LiB + MB
5	1.0862	1.3480	4.11	0.99	0.27	94.63	84.26	10.52	5.22	18207	LiB + MB
6	1.0867	1.3489	4.02	1.58	0.27	94.13	78.92	16.09	4.99	17343	LiB + MB
7	1.0866	1.3490	3.99	2.24	0.25	93.52	74.07	21.56	4.37	16292	LiB + MB
8	1.0887	1.3498	3.71	2.37	0.28	93.64	71.31	23.62	5.07	16891	LiB + MB
9	1.0958	1.3510	3.54	3.00	0.28	93.18	66.06	29.02	4.92	16317	LiB + MB
10	1.1006	1.3523	3.65	3.74	0.25	92.36	62.67	33.29	4.04	14881	LiB + MB
11	1.1091	1.3526	3.73	4.33	0.25	91.69	60.06	36.15	3.79	13855	LiB + MB
12, E	1.1186	1.3535	3.63	4.87	0.25	91.25	56.80	39.51	3.69	13400	LiB + MB + RB
13, B	1.1415	1.3472	3.61	4.46	0.00	91.93	60.96	39.04	0.00	14567	LiB + RB
14, E	1.1186	1.3535	3.63	4.87	0.25	91.25	56.80	39.51	3.69	13400	LiB + MB + RB
15, C	1.1140	1.3414	0.00	3.86	0.38	95.76	0.00	84.83	15.17	38092	MB + RB
16	1.1042	1.3435	0.10	3.83	0.37	95.70	4.11	81.57	14.32	36895	MB + RB
17	1.1077	1.3442	0.22	3.82	0.34	95.62	8.73	78.57	12.70	35598	MB + RB
18	1.1048	1.3449	0.42	3.84	0.27	95.47	15.76	74.70	9.54	33616	MB + RB
19	1.1082	1.3452	0.61	3.89	0.27	95.23	21.17	70.00	8.83	31019	MB + RB
20	1.1049	1.3459	0.87	3.95	0.25	94.93	27.59	64.94	7.47	28251	MB + RB
21	1.1096	1.3491	1.70	4.84	0.20	93.26	38.66	57.06	4.28	19901	MB + RB
22	1.1048	1.3499	2.12	4.88	0.24	92.76	43.48	51.88	4.64	17852	MB + RB
23	1.1055	1.3502	2.97	4.91	0.19	91.93	52.15	44.70	3.15	15150	MB + RB
24, E	1.1186	1.3535	3.63	4.87	0.25	91.25	56.80	39.51	3.69	13400	LiB + MB + RB

[a] Standard uncertainties u are $u(T) = 0.20$ K; $u_r(p) = 0.05$; $u_r(\rho) = 2.0 \times 10^{-4}$ g cm^{-3}; $u_r(n) = 1.0 \times 10^{-4}$; $u_r(Li_2B_4O_7) = 0.0050$; $u_r(Rb_2B_4O_7) = 0.0050$; $u_r(MgB_4O_7) = 0.0050$; LiB–$Li_2B_4O_7 \cdot 3H_2O$, RB–$RbB_5O_8 \cdot 4H_2O$, MB–$MgB_4O_7 \cdot 9H_2O$.

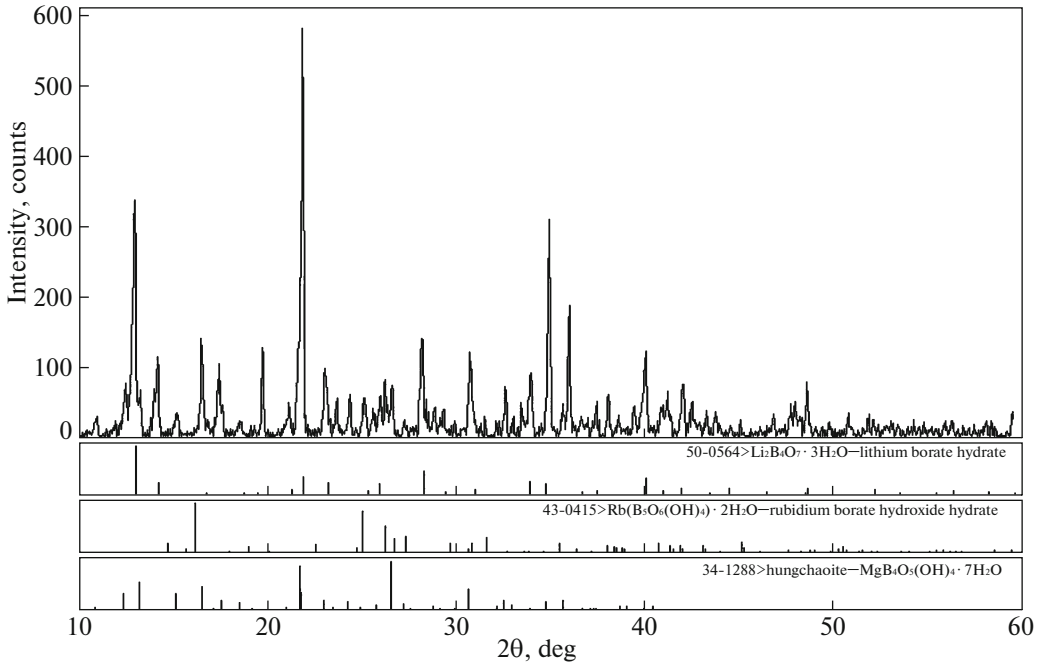

Fig. 2. X-ray diffraction pattern of the invariant point E in the quaternary system Li^+,Rb^+,Mg^{2+}//borate–H_2O at 323 K.

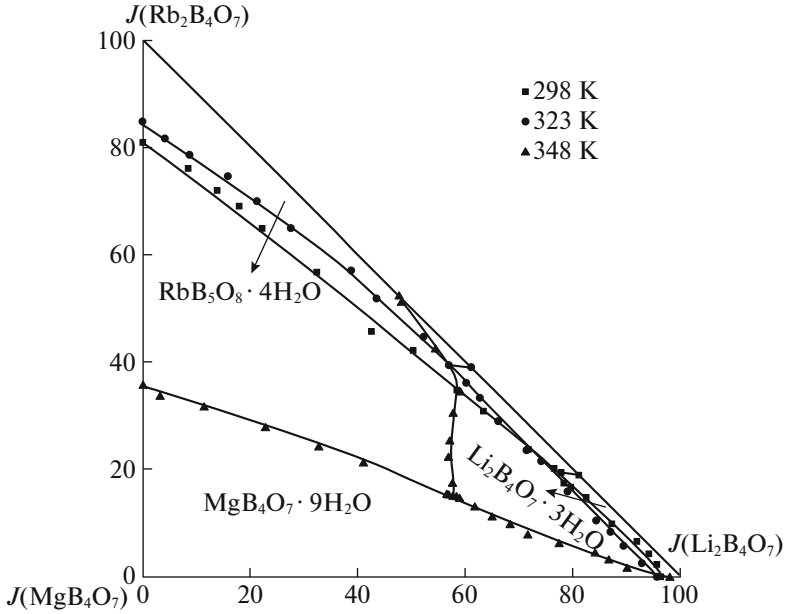

Fig. 3. Phase diagram of quaternary system Li^+,Rb^+,Mg^{2+}//borate–H_2O at 298, 323, and 348 K (■ 298 K [12], ● 323 K, ▲ 348 K [13]).

298 and 348 K, the crystalline area of $RbB_5O_8 \cdot 4H_2O$ is the smallest than that of 298 and 348 K, while the crystalline are of $Li_2B_4O_7 \cdot 3H_2O$ is larger than that of 298 K, while smaller than that of 348 K.

Figures 4–6 were constructed with $J(Rb_2B_4O_7)$ as the abscissa and $J(H_2O)$, the density, or the refractive index of the solution at equilibrium as the ordinate. As Fig. 4 shows, the water content decreases on the AE

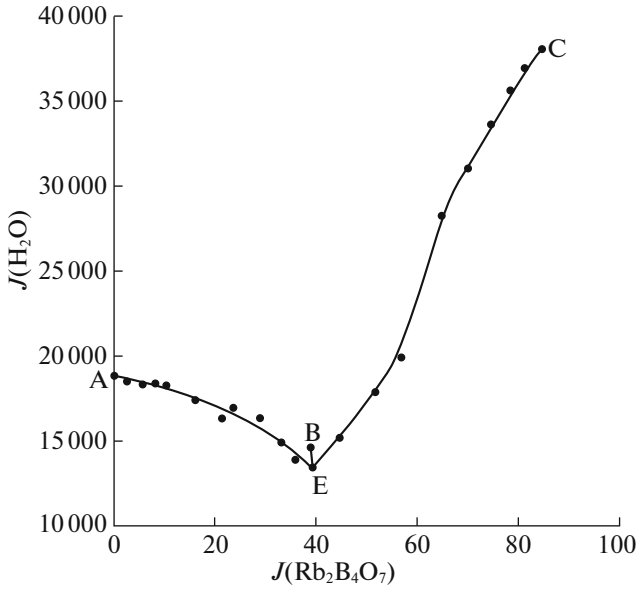

Fig. 4. Water-content diagram of Li^+,Rb^+,Mg^{2+}//borate–H_2O at 323 K.

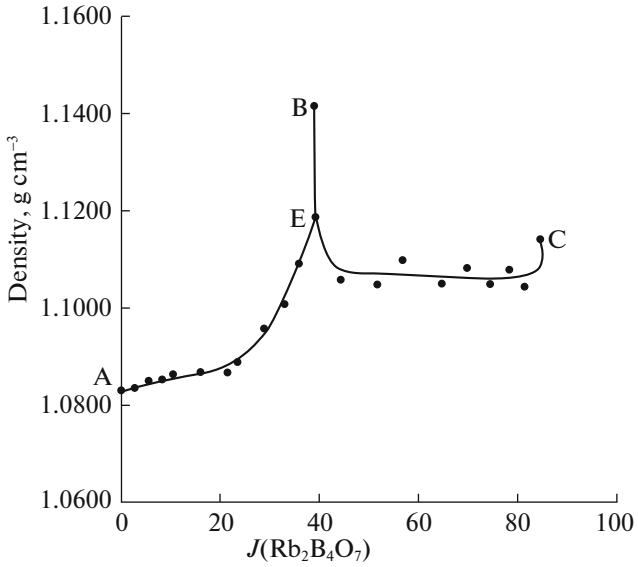

Fig. 5. Densities vs composition diagram of Li^+,Rb^+,Mg^{2+}//borate–H_2O at 323 K.

and BE curve with $J(Rb_2B_4O_7)$ incrementally until it reaches the smallest value at point E; while, on the curve CE, the water content reduces with $J(Rb_2B_4O_7)$ decrement until it reaches the smallest value at point E. Figures 5 and 6 show that on the monovariant curve AE, the values of density and refractive index of the solution at equilibrium are positively correlated with $J(Rb_2B_4O_7)$, the refractive indices increase along with $J(Rb_2B_4O_7)$ decrease on the curves BE and CE, and reach the maximum values at invariant point E.

5. CONCLUSIONS

The solubilities and physicochemical properties (density and refractive index) of the aqueous quaternary system Li^+,Rb^+,Mg^{2+}//borate–H_2O at 323 K were investigated by using the isothermal dissolution method. The solid phases of the quaternary system were $Li_2B_4O_7 \cdot 3H_2O$, $MgB_4O_7 \cdot 9H_2O$, and $RbB_5O_8 \cdot 4H_2O$. It is found that $MgB_4O_7 \cdot 9H_2O$ salt contains almost of the crystallization field. Comparisons between the stable phase diagrams at 298, 323, and 348 K show that the crystalline form of three salts was not affected by temperature from 298 to 348 K, when the temperature is 323 K, the crystalline are of $MgB_4O_7 \cdot 9H_2O$ is the largest than that of 298 and 348 K, the crystalline area of $RbB_5O_8 \cdot 4H_2O$ is the smallest, the crystalline are of $Li_2B_4O_7 \cdot 3H_2O$ is larger than that of 298 K, while smaller than that of 348 K.

ACKNOWLEDGMENTS

Supported by the National Natural Science Foundation of China (U1507111, 41473059), the Research Fund from the Science and Technology Department of Sichuan Province (2017JY0191).

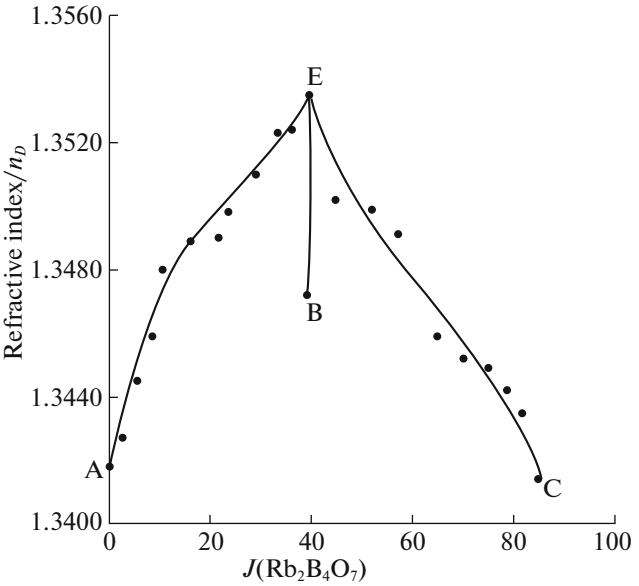

Fig. 6. Refractive indices vs. composition diagram of Li^+,Rb^+,Mg^{2+}//borate–H_2O at 323 K.

REFERENCES

1. J. Li and S. Y. Gao, J. Salt Lake Sci. **1**, 62 (1993).
2. S. Feng, X. D. Yu, X. L. Cheng, and Y. Zeng, Russ. J. Phys. Chem. A **91**, 2149 (2017).
3. X. D. Yu, M. Liu, L. Wang, X. L. Cheng, and Y. Zeng, J. Chem. Eng. Chin. Univ. **32**, 514 (2018).
4. A. V. Churikov, K. V. Zapsis, V. V. Khramkov, M. A. Churikov, and I. M. Gamayunova, J. Chem. Eng. Data **56**, 383 (2011).
5. L. Li, Y. F. Guo, S. S. Zhang, M. M. Shen, and T. L. Deng, Fluid Phase Equilib. **436**, 13 (2017).
6. L. Z. Meng and D. Li, Braz. J. Chem. Eng. **31**, 251 (2014).
7. X. D. Yu, Y. L. Luo, L. T. Wu, X. L. Cheng, and Y. Zeng, J. Chem. Eng. Data **61**, 3311 (2016).
8. S. S. Guo, X. D. Yu, and Y. Zeng, J. Chem. Eng. Data **61**, 1566 (2016).
9. X. D. Yu, Y. Zeng, P. J. Chen, and L. G. Li, J. Chem. Eng. Data **63**, 3125 (2018).
10. S. Turesunbadalov and L. Soliev, J. Chem. Eng. Data **63**, 598 (2018).
11. X. D. Yu, Y. Zeng, S. S. Guo, and Y. J. Zhang, J. Chem. Eng. Data **61**, 1246 (2016).
12. X. Duan, Y. Zeng, J. Luo, Y. Tao, and X. D. Yu, J. Chem. Eng. Jpn. **50**, 470 (2017).
13. H. B. Li, L. Liu, X. D. Yu, Y. J. Zhang, Z. Q. Li, and Y. Zeng, Russ. J. Phys. Chem. A **89**, 1572 (2015).
14. Y. Zeng, X. D. Yu, L. L. Liu, and Q. H. Yin, CN Patent No. 103172078 A (2013).
15. Y. Jing, Sea-Lake Salt Chem. Ind. **29**, 24 (2000).
16. H. Y. Cheng and H. Cheng, *Chemical Reagent-General Methods for the Determination of Density* (China Standards Press, Beijing, 2007).
17. H. Z. Yuan, Y. J. Zhu, L. P. Wu, and X. Zhang, Rock Miner. Anal. **30**, 87 (2011).
18. Inst. of Qinghai Salt-Lake, Chin. Acad. Sci., *Analytical Methods of Brines and Salts* (Science Technol. Press, Beijing, 1984).